

Physical content of electron-charge-density distributions in *A15* compounds

J.-L. Staudenmann

Ames Laboratory and Department of Physics, Iowa State University, Ames, Iowa 50011

B. DeFacio

Department of Physics, University of Missouri at Columbia, Columbia, Missouri 65211

C. Stassis

Ames Laboratory and Department of Physics, Iowa State University, Ames, Iowa 50011

(Received 2 July 1982; revised manuscript received 12 November 1982)

The starting point of the present article is a careful analysis of the physical meaning of the three deformation electron-charge-density maps for V_3Si , V_3Ge , and Cr_3Si [previously presented by J.-L. Staudenmann *et al.*, Phys. Rev. B **24**, 6446 (1981)]. Based on the significant differences exhibited in these maps, it was shown that one can organize all the Debye temperatures at 0 K from specific-heat measurements into five collections which were called *Debye classes*. The findings here presented are not limited to *A15* alloys alone, but rather can be applied to any other family of compounds that satisfies the free-atom superposition principle and the small-amplitude vibration hypothesis. It is shown that deformation electron charge densities depend only weakly upon structure and that they are mainly related to physical properties. Furthermore, the use of deformation electron-charge density as a criterion in setting the starting point for the three main Debye classes is justified *a posteriori*. We point out that when one takes into account the consequences of the dielectric function, the static or bonding electron charge density can only be extracted with great difficulty from any experimental data. This certainly complicates any comparison between experimental and computed electron charge densities. It is shown that the deformation and total electron charge densities are the only well-defined inverse Fourier transforms. If the vibration amplitude of the valence-electron orbitals are non-negligible, the valence-electron charge density, in contrast to the deformation and total electron charge densities, has no simple interpretation. It has the same meaning, however, if the valence-electron orbitals are in a quasi-static configuration. Moreover, in the case of a non-negligible vibration amplitude for the valence-electron orbitals, the comparison between valence- and deformation-electron charge densities leads to a qualitative separation between dynamics and statics for the valence-electron orbitals. This observation is of fundamental importance in linking experimental electron charge densities and inelastic neutron scattering measurements.

I. INTRODUCTION

In this article we consider x-ray diffraction techniques for the study of the variations of the electron-charge-density distributions (abbreviated as ECD in the text and defined in Sec. II). Any diffraction experiment consists of measuring the Fourier transform of a value proportional to a density. In the case of x-ray diffraction, the density is that of the charge of the electrons in the unit cell, and the Fourier transform of this density is represented by an *infinity* of Bragg peak intensities. The ECD distribution is then achieved by means of

the inverse Fourier transform of all observed structure factors. The larger the set of experimental Bragg peaks included in the inversion process, the smaller the truncation errors will be. The fundamental problems of the finite inverse Fourier transform are clearly and comprehensively discussed in the article of Auslander and Tolimieri,¹ whereas a *tour de force* on the relations between harmonic analysis and symmetry are given by Mackey.²

In the case of difference ECD maps one sees primarily the location of the valence electrons which hold the atoms together. In addition, the ECD maps also reflect the vibrations of the valence electrons superimposed on their static distribution. This

vibrational effect on the static ECD is a *smearing* of the static ECD. By static ECD we mean ECD distributions containing the bonding information alone. It is well known that the vibrations of the atoms are temperature dependent, and so is the smearing of the ECD distributions. This means that the static ECD can only be approached at a temperature where the smearing effects are minimized. Coppens³ basically proposed to use the lowest accessible temperature in all cases. This, in fact, is valid only for normal solids because the vibrations of the atoms are *harmonically* reduced when the temperature is lowered: The vibrations harden without any significant anharmonic contributions. In order to choose the temperatures at which the smearing effects are minimized, one must assess the temperature factors and thermodynamic properties very carefully,⁴ or, in a cruder way, discuss the various domains that can be seen on a plot of the Debye temperature as a function of the temperature as given from specific measurements⁵ or from sound velocity measurements (see Ref. 6 and Fig. 1). In this type of plot, a normal solid shows a very slow, steadily decreasing curve when the temperature is increased. In the latter approach, one can use Fig. 1 concerning V_3Si (Ref. 6) to illustrate the various temperature settings.

One of the purposes of this article is to show that the smearing of the ECD's provides information about the dynamics of the valence electrons as well as about chemico-physical properties weakly dependent upon the structure. In the range where the latter properties are constant or very slowly varying, the dynamics of the valence electrons might be assessed by making differences between two difference densities at two different values of a physical constraint. By physical constraint we mean a temperature variation, or a pressure change, or the application of a magnetic field, etc. A chemical constraint would be a concentration change within an homogeneity domain, or the controlled adjunction of impurities (like hydrogen) in a host matrix (as hcp scandium). All of these constraints are at our disposal to modify in different ways the ECD distributions within the unit cell of interest.

Three final introductory comments: (a) We assume that the various corrections such as Lorentz and polarization effects as well as absorption and extinction have been done properly beforehand. Thus they will not be discussed in the present article. (b) The present study does not take into account physical effects which can arise when doing diffraction experiments in the vicinity of absorption edges. (c) Detailed procedure and results concerning the analysis of the thermal parameters will be published elsewhere.⁷

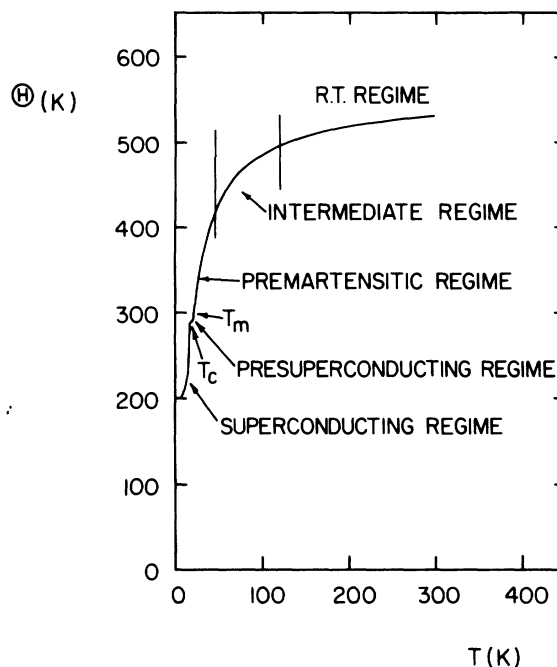


FIG. 1. Plot of the Debye temperature as a function of the temperature for V_3Si from Ref. 6 as determined from sound velocity measurements on single crystals (courtesy of Dr. L. R. Testardi). The descriptions of the five temperature ranges are as follows. (a) $T > 120$ K or room-temperature regime. Although this range already exhibits a softening—opposite behavior to the one described in the text for normal solids—the smearing effects are probably minimized at ~ 120 K with respect to the one at 300 K. (b) $50 > T > 120$ K or intermediate regime. Based on Ref. 30 and Table III, anharmonicity is beginning to play a significant role at ~ 120 K in the dynamics of the valence electrons. Consequently, until diffraction experiments are done in this range, the best temperature setting in determining the static ECD remains an open question. (c) $22 > T > 50$ K or premartensitic regime. In this range ~ 50 K is probably the temperature which should minimize the smearing effects because ~ 22 K represents the temperature at which the martensitic transition takes place. (d) $17 > T > 22$ K or presuperconducting regime. This regime is probably the most erratic of all and no guesses are possible here since the two transitions are probably related. An interesting test for coupling and competition between the two transitions should be performed in Nb_3Sn where they are farther apart: ~ 45 and 18 K, respectively (Ref. 41). (e) $T < 17$ K or superconducting regime. Here, clearly, the lowest possible temperature is the one which will minimize the smearing effects. This does not mean, however, that this temperature can be conceded for all of the above regimes, because ECD distributions are not only significantly different from the ones at room temperature but also exhibit a different type of ECD (Ref. 33). Similar comments can be made on Si and Ge (Ref. 5).

II. ELECTRON-CHARGE DENSITIES

The density of the electron charges $\rho(\omega, \vec{r})$ at a location \vec{r} within the unit cell, at a given temperature T , and other external conditions can be written as

$$\rho(\omega, \vec{r}) = \frac{1}{V} \sum_{h=-\infty}^{\infty} \sum_{k=-\infty}^{\infty} \sum_{l=-\infty}^{\infty} F(\omega, \vec{H}) \times \exp(-2\pi i \vec{H} \cdot \vec{r}) . \quad (1)$$

The ω dependence is kept to indicate that the measurement has been done at a given frequency and that some electronic effects might be frequency dependent. Here V is the volume of the unit cell; h, k, l are the Miller indices defining the static reciprocal vector \vec{H} such that $\vec{H} = h \vec{a}^* + k \vec{b}^* + l \vec{c}^*$ where \vec{a}^* , \vec{b}^* , and \vec{c}^* are the unit-cell reciprocal vectors. $F(\omega, \vec{H})$ is the structure factor and its value can be obtained by Fourier transforming Eq. (1):

$$F(\omega, \vec{H}) = V \int_{x=0}^1 \int_{y=0}^1 \int_{z=0}^1 \rho(\omega, \vec{r}) \times \exp(2\pi i \vec{H} \cdot \vec{r}) d^3r , \quad (2)$$

where $d^3r = dx dy dz$. Equation (2) is too complicated for practical computation. Furthermore, one cannot use

$$\rho(\omega, \vec{r}) = \sum_n \rho_{\text{core},n}(\omega, \vec{r}) + \rho_{\text{val}}(\omega, \vec{r}) , \quad (3)$$

where the summation represents the superposition of the electron cores and $\rho_{\text{val}}(\omega, \vec{r})$ is the valence ECD of all valence electrons in the unit cell, because $\rho_{\text{val}}(\omega, \vec{r})$ needs a true and realistic electronic structure calculation to be properly computed. Therefore Eq. (2) is simplified once more by using the simple superposition of the free spherical atoms forming the unit cell⁸:

$$F(\omega, \vec{H}) = \sum_n f_n(\vec{H}) \exp(2\pi i \vec{H} \cdot \vec{x}_n) T_n(\omega, \vec{H}) , \quad (4)$$

where n is the index running through all the atoms shaping the unit cell, $f_n(\vec{H})$ is the scattering factor of the n th atom usually computed for a spherical distribution of the electrons around the nuclei^{9,10}; \vec{x}_n is the position vector indicating the exact crystallographic location of the n th atom; $T_n(\omega, \vec{H})$ is the thermal parameter or Debye-Waller factor of the n th atom. The superposition of free atoms has the advantage of the *simplicity* but, unfortunately, it does not account for electronic anisotropies. They affect the electronic shells around atoms, including core polarizations, created by bonding and by charge transfers between atoms (see below).

A given structure is represented by a unique set of Bragg reflections. Each compound belonging to this particular structure is characterized by intensity changes within the set of Bragg reflections. The uniqueness of the inverse Fourier transform is only valid for centrosymmetric structures.⁸ Therefore the following, as well as future studies, will be strictly limited to materials with centrosymmetric structures. Three main inverse Fourier transforms are usually discussed.

A. Total electron-charge density

One has

$$\rho_{\text{tot}}(\omega, \vec{r}) = \frac{1}{V} \sum_{\vec{H}} F_{\text{obs}}(\omega, \vec{H}) \exp(-2\pi i \vec{H} \cdot \vec{r}) , \quad (5)$$

where $F_{\text{obs}}(\omega, \vec{H})$ represents the experimental data. This ECD must be positive in the complete unit cell. It reveals extremely strong peaks at the locations of the atomic positions. But, owing to the magnitude of these atomic peaks, small deformations indicating bonds and/or asphericities in the immediate surroundings of the atoms are impossible to see. Therefore this well-defined inverse Fourier transform is mainly used for structure determination.

B. Valence electron-charge density

One has

$$\rho_{\text{val}}(\omega, \vec{r}) = \frac{1}{V} \sum_{\vec{H}} [F_{\text{obs}}(\omega, \vec{H}) - F_{\text{core}}(\omega, \vec{H})] \times \exp(-2\pi i \vec{H} \cdot \vec{r}) , \quad (6)$$

where, according to Eq. (4), one can write

$$F_{\text{core}}(\omega, \vec{H}) = \sum_n f_{\text{core},n}(\vec{H}) \times \exp(2\pi i \vec{H} \cdot \vec{x}_n) T_n(\omega, \vec{H}) \quad (7)$$

with $f_{\text{core},n}(\vec{H})$ being the scattering factor (or "form" factor) for the core electron of the n th atom (see Fig. 2 for V_{core} , for instance and see Figs. 6 and 8 as examples of valence ECD's). This ECD, contrary to the previous one, does reveal deformations with respect to spherical atom electron cores. It is mainly a positive density in the whole unit cell unless the core-electron shell has been deformed by bonding or by some other excitations. It allows an easy detection of delocalized electrons as well as any deformation from spherical symmetry.

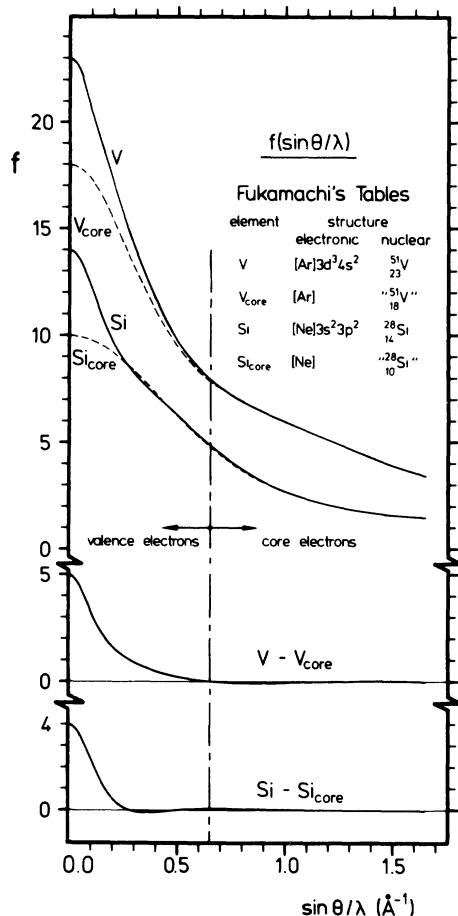


FIG. 2. Plot of the number of electrons responsible for the scattering process as a function of the momentum transfer expressed in terms of $\sin\theta/\lambda$. The examples shown here are vanadium and silicon taken from Fukamachi (Ref. 9). The upper curve represents the scattering from the vanadium electrons while the lower curve indicates the scattering from the silicon electrons. The dashed curves show the scattering from the core electrons. The differences between two curves corresponding to one atom are the effects of the valence electrons for this atom. For $\sin\theta/\lambda > 0.7 \text{ \AA}^{-1}$ there are fluctuations in these differences which are very difficult to assess by the experiment (see Table I). Consequently, by cutting the inverse Fourier transform in the vicinity of the beginning of these fluctuations, details around atomic sites are neglected while the details in the surroundings of the bonds are emphasized.

C. Deformation electron-charge density

One has

$$\rho_{\text{def}}(\omega, \vec{r}) = \frac{1}{V} \sum_{\vec{H}} [F_{\text{obs}}(\omega, \vec{H}) - F_{\text{spher}}(\omega, \vec{H})] \times \exp(-2\pi i \vec{H} \cdot \vec{r}), \quad (8)$$

where, according to Eq. (4), one has

$$F_{\text{spher}}(\omega, \vec{H}) = \sum_n f_n(\vec{H}) \times \exp(2\pi i \vec{H} \cdot \vec{x}) T_n(\omega, \vec{H}) \quad (9)$$

with $f_n(\vec{H})$ being the scattering factor for all the electrons of the n th atom (see Fig. 2 for V taken as an example). $f_{\text{core},n}(\vec{H})$ and $f_n(\vec{H})$ are usually computed for spherical symmetry and given in the form of tables.^{9,10} As a consequence, the two above difference ECD's mainly exhibit the delocalization of the valence electrons with respect to an hypothetical spherical symmetry distribution of the electrons around the atomic positions. (See Figs. 7 and 9–11 as examples of deformation ECD's.) In "perfect" cases—that is, when extinction, scale factor, and other corrections can be properly applied—the deformation ECD must be slightly negative at the atomic positions. It also allows easy detection of any asphericities around atomic positions as well as the locations of bonding electrons. It is also used to locate hydrogen atoms. Like the total ECD, the deformation ECD is a well-defined density in any circumstance.

D. Valence versus deformation ECD

These two are complementary when the valence orbitals are in quasistatic configurations. In these cases they cannot contradict one another. We shall see below that the knowledge of each leads to fundamental insights into the dynamics of the valence electron orbitals. Since x rays are diffracted by all electrons, it is only possible to deduce experimental form factors $f_n(\vec{H})$ [see Ref. 11(a)] from the observed structure factors $F_{\text{obs}}(\omega, \vec{H})$.

E. Errors in electron charge density distributions

In x-ray diffraction, diffracted intensities result from all the electrons occupying a unit cell. Consequently, the errors in ECD maps reflect the errors (or standard deviations) of all the crystallographic variables applied to all the electrons occupying the unit cell. Hence the magnitude of the densities at the nuclear positions are found to be very important for the $A15$ compounds and so are the errors at these particular points where all error contributions accumulate. Rees¹² initiated a computation of errors in ECD maps, and Table I shows how large these errors can be at the atomic positions.

On reanalyzing the V_3Si experimental data,¹³ Ho¹⁴ found humps located at $\sim 0.25 \text{ \AA}$ on each side of the V sites in agreement with the theoretical result of Mattheiss and Hamann.¹⁵ These humps, however,

TABLE I. Computed ECD errors in $e \text{ \AA}^{-3}$ for V_3Si (Refs. 13 and 33) and for Cr_3Si (Ref. 34) according to the procedure published by Rees (Ref. 12). The various measurements on V_3Si were of comparable quality and consequently the V_3Si column is valid for the 13.5 and 300 K sets of data. A represents either the V or the Cr atom and “ $A-I-A$ ” designates the middle point between two consecutive A atoms on a chain.

	Cr_3Si ($e \text{ \AA}^{-3}$)	V_3Si ($e \text{ \AA}^{-3}$)
A atom	6.5	7
A atom + 0.35- \AA radius	0.08	0.1
$A-I-A$	0.08	0.1
Si atom	4.3	4.5
Si atom + 0.3- \AA radius	0.08	0.1
Everywhere else	0.04	0.05

fall within the errors (see Table I) and, consequently, *cannot* be experimentally proven by ECD methods alone. But Ho’s work definitely ruled out the possibility that these humps can be found as far as $\sim 0.55 \text{ \AA}$ from the V sites as computed by Lam and Cohen.¹⁶ Experimentally, comparisons between computed and observed ECD’s can only be made at distances greater than $\sim 0.4 \text{ \AA}$ from any nuclear position whereas, from the band theory point of view, the comparison should be made within a radius of $\sim 0.5 \text{ \AA}$.

III. DIELECTRIC FUNCTION OF CRYSTALS

A. Preliminaries

This section is devoted to the connection between ECD’s and the generalized electronic susceptibility function $\chi(\omega, \vec{H})$. According to Ashcroft and Mermin¹⁷ and Madelung,¹⁸ the limit $\chi(\omega, \vec{0})$ describes collective excitations such as phonon modes and surface plasmons. This limit is a justification for small-angle scattering experiments. The other extreme, $\chi(0, \vec{H})$, describes the electrostatic screening of the electron-electron, electron-lattice, and electron-impurity interactions in crystals. This second limit is difficult to envision without extrapolation in diffraction experiments, because one always measures $\chi(\omega, \vec{H})$ at constant ω .

When discussing all of the known $A 15$ alloys, it is not possible to use any single approximation for the entire family. It is necessary in many cases to treat the electron-electron and electron-phonon interactions together. Under some conditions, such as narrow bands with wide gaps or broad bands with nar-

row gaps, approximations can be made where electron-electron and the electron-phonon interactions can be treated separately (Mahan¹⁹). It seems that most of the $A 15$ compounds have broad bands with narrow gaps, but the thermal properties are so widely different that no single approximation can describe all of these differences.²⁰ The connections between $\chi(\omega, \vec{H})$ and x-ray diffraction have been developed by James²¹ and by Batterman and Cole,²² but these two articles are restricted to the static first term in the expansion. In the following, discussions of more general cases are presented.

Crystals are three-dimensional periodic arrays of atoms. The core-electron orbitals are distributed around the nuclei with small departures from spherical symmetry distributions. On the other hand, the valence ECD is highly anisotropic because of bonding and contributions from physical effects. In the case of alloys, chemical differences among components may also appear in the valence ECD. This can be expressed in terms of a dielectric function which can be written as an inverse Fourier transform over the reciprocal lattice is exactly the same manner as that of the ECD’s. In a future article,²³ we plan to show how the dielectric susceptibility formalism applies to present sets of data to give a microscopic description of the processes under discussion.

B. Dielectric function of the electron gas

In the following, we neglect surface effects such as changes in the phase of the x-ray wave. The surface consists of a few atomic layers (about 10 \AA) compared with spherical crystals of $\sim 10^6 \text{ \AA}$ in diameter. This implies that the various effects which are due to the surface of the sample, such as x-ray photoemission, and which are translated by the photoemission, and represented by a structure factor $F_{\text{surface}}(\omega, \vec{H})$ can be neglected as well as the corresponding ECD. Note that the following treatment can be started in the reciprocal space as well as in the direct space; we have chosen to follow the route of James²¹ and Batterman and Cole.²²

The incident x-ray beam carries on an electric field $\vec{E}(\omega, \vec{H})$ which induces an electric displacement field $\vec{D}(\omega, \vec{H})$. In the hypothesis of small electronic displacements the field $\vec{D}(\omega, \vec{H})$ can be written as

$$\begin{aligned} \vec{D}(\omega, \vec{H}) &= \epsilon_0 \vec{E}(\omega, \vec{H}) + \vec{P}(\omega, \vec{H}) \\ &= \chi(\omega, \vec{H}) \epsilon_0 \vec{E}(\omega, \vec{H}), \end{aligned} \quad (10)$$

where ϵ_0 is the permittivity of the vacuum. $\chi(\omega, \vec{H})$ is the dielectric function or relative permittivity; it is a tensor of rank 2: that is, \vec{D} and \vec{E} need not be colinear. $\vec{P}(\omega, \vec{H})$ is the polarization per unit volume

of the crystal, that is, a polarization density. As the core electron orbitals exhibit an almost spherical symmetry and also because they are locked in by the Pauli exclusion principle, their contributions to $\vec{P}(\omega, \vec{H})$ can be neglected and, therefore,

$$\begin{aligned} \vec{P}(\omega, \vec{H}) &\sim - \sum_j^{\text{valence}} e \vec{H} \\ &\sim - \frac{e^2 N_{\text{val}} \vec{E}(\omega, \vec{H})}{m \omega^2} \end{aligned} \quad (11)$$

is certainly valid for most of the atoms with the exception, perhaps, of the ones occupying the first two rows of the Periodic Table (N_{val} is the total number of valence electrons in a unit volume of the substance²⁴). Furthermore, Eq. (10) leads to

$$\begin{aligned} \text{div} \vec{D}(\omega, \vec{H}) &\propto \text{div} [\chi(\omega, \vec{H}) \epsilon_0 \vec{E}(\omega, \vec{H})] \\ &\propto \frac{1}{\epsilon_0} F_+(\omega, \vec{H}) \end{aligned} \quad (12)$$

and

$$\text{div} \vec{E}(\omega, \vec{H}) \propto \frac{1}{\epsilon_0} [F(\omega, \vec{H}) + F_+(\omega, \vec{H})], \quad (13)$$

where $F_+(\omega, \vec{H})$ is the form factor due to all possible effects contained in the susceptibility function as listed above.²⁴ By Fourier transforming Eq. (13), one gets

$$\begin{aligned} \text{div} \vec{E}(\omega, \vec{r}) &= \text{div} \left[\sum_{\vec{H}} \vec{E}(\omega, \vec{H}) \exp(-2\pi i \vec{H} \cdot \vec{r}) \right] \quad (14a) \\ &\propto \frac{1}{\epsilon_0} \sum_{\vec{H}} [F(\omega, \vec{H}) + F_+(\omega, \vec{H})] \\ &\quad \times \exp(-2\pi i \vec{H} \cdot \vec{r}) \\ &\propto \frac{1}{\epsilon_0} [\rho(\omega, \vec{r}) + \rho_+(\omega, \vec{r})], \end{aligned} \quad (14b)$$

where $\rho_+(\omega, \vec{r})$ is the ECD due to $F_+(\omega, \vec{H})$. Equation (14b) is very important because it shows that *any experimental ECD is a superposition of static ECD plus dynamical and correlation effect ECD's*. Similarly the Fourier transform of Eq. (12) gives

$$\text{div} \vec{D}(\omega, \vec{r}) = \text{div} \left[\sum_{\vec{H}} \chi(\omega, \vec{H}) \vec{E}(\omega, \vec{H}) \exp(-2\pi i \vec{H} \cdot \vec{r}) \right] \quad (15a)$$

$$\begin{aligned} &\propto \frac{1}{\epsilon_0} \sum_{\vec{H}} F_+(\omega, \vec{H}) \exp(-2\pi i \vec{H} \cdot \vec{r}) \\ &\propto \frac{1}{\epsilon_0} \rho_+(\omega, \vec{r}). \end{aligned} \quad (15b)$$

In each case the proportional factor contains $1/V$ where V is the volume of the unit cell. The Eqs. (14) and (15) must be satisfied term by term. Therefore, dividing one by the other one gives

$$\chi(\omega, \vec{H}) = \frac{F_+(\omega, \vec{H})}{F(\omega, \vec{H}) + F_+(\omega, \vec{H})} \quad (16)$$

and

$$\chi(\omega, \vec{r}) = \frac{\rho_+(\omega, \vec{r})}{\rho(\omega, \vec{r}) + \rho_+(\omega, \vec{r})}.$$

These relations show that it is possible, in principle, to extract $\chi(\omega, \vec{r})$ from ECD maps when a physical constraint is applied because $\rho_+(\omega, \vec{r})$ is modified by it. In a subsequent article²³ we plan to show what excitation types are needed in order to extract useful physical information from the $F_+(\omega, \vec{H})$ or the $\rho_+(\omega, \vec{r})$. Our present goal is not to discuss in detail all of the effects described in Sec. III A but to point out that they are all present in ECD maps.

In any x-ray diffraction experiment the valence electrons are more or less close to a resonance state with the x-ray frequency. This means that the ω dependence of most of the above relations is more complicated than it seems at first sight. Instead of a proper analysis of the real and imaginary parts of $\chi(\omega, \vec{H})$ (see, for instance, Madelung¹⁸), this is translated in x-ray work by considering the structure factors and, consequently, the form factors as complex and wavelength dependent: $f_n(\vec{H}) + \Delta f_n'(\lambda) + i \Delta f_n''(\lambda)$, where $\Delta f_n'(\lambda)$ is the real part of the form factor and correction due to the proximity of the resonance for the n th atom, and $\Delta f_n''(\lambda)$ is the form factor correction due to absorption phenomena near the edge of the n th atom.

IV. CONNECTIONS BETWEEN PHYSICAL AND CRYSTALLOGRAPHIC APPROACHES

From the ECD's at room temperature shown in Ref. 20 for the $A15$ alloys V_3Si , V_3Ge , and Cr_3Si , one can easily see that these three ECD's present three different types of ECD within the $A15$ crystal structure. The matter discussed there is based on the assumption that these various types of ECD are related in complicated ways to the physical properties such as anharmonicity and, to a lesser extent, to the superconducting transition temperature.²⁰ The variations of the magnetic susceptibilities as a function of the temperature for the above three compounds^{25,26} also seem to agree with the hypotheses of Ref. 20. In other words, interactions between atoms are not only responsible for the crystal structure but are also important aspects of the physical properties.

TABLE II. Selection of x-ray single-crystal *harmonic* vibrational amplitudes to show that the small vibration amplitude hypothesis is reasonable even if perturbative anharmonicity contributions may double or triple the percentage given in column 6. Column 2 indicates the percentage of valence electrons with respect to the number of core electrons. The \sim sign means that a chemical average has been made on the vibrations of the various atoms composing the unit cell along the main axes. Numbers between parentheses are the standard deviations for the last digit of the main preceding number. The (*) sign means that the room-temperature lattice parameter has been used to compute the vibration percentage.

Metal or compound	Valence/ core electron ratio (%)	T (K)	Lattice constants a and c (Å)	Mean atomic Harmonic vibration (Å)	Ratio of the mean atomic vibration to the lattice constant (%)	Reference
Be	100	300	$a = 2.2858(2)$ $c = 3.5843(3)$	0.087 0.083	3.80 2.31	11(a)
Cr	33	300	$a = 2.8841(1)$	0.064	2.21	58
Cu	4	50	$a = 3.60350(5)$	0.046	1.38	59
		300	$a = 3.61496(2)$	0.087	2.41	60
Graphite	200	300	$a = 2.461(4)$ $c = 6.706(2)$	~ 0.056 ~ 0.118	~ 2.28 ~ 1.76	61
Ho	24	300	$a = 3.5773$ $c = 5.6158$	0.110 0.111	3.09 1.97	62
Si	40	92.2 293.2	$a = 5.43044$	0.054 0.076	0.99 (*) 1.41	63
V	28	300	$a = 3.0257(4)$	0.087	2.88	64
AlN	67	300	$a = 3.1114$ $c = 4.9792$	~ 0.060 ~ 0.60	~ 1.91 ~ 1.20	65
Cr ₃ Si	34	300	$a = 4.564$	~ 0.061	~ 1.33	34
MgF ₂	114	300	$a = 4.628(5)$ $c = 3.045(3)$	~ 0.087 ~ 0.075	~ 1.87 ~ 2.46	66
MgSn ₂	10	300	$a = 6.7638$	~ 0.105	~ 1.56	67
Nb ₃ Sn	12	300	$a = 5.294$	~ 0.072	~ 1.36	68
TiC	40	300	$a = 4.328$	~ 0.067	~ 1.54	69
V ₃ Ge	19	300	$a = 4.782$ $a = 4.783$	~ 0.071 ~ 0.072	~ 1.49 ~ 1.51	68 70
V ₃ Si	30	13.5 78 300	$a = 4.719(2)$ $a = 4.718(1)$ $a = 4.7240(5)$	~ 0.043 ~ 0.057 ~ 0.074	~ 0.91 ~ 1.21 ~ 1.56	33 70 13,33

In this section we bridge the physical description of a system with its crystallographic approach; that is, we connect the collective modes approach (see below) with the vibrations of individual atoms linked by the symmetries of the system. In doing so we like to follow the clear discussion of Reif²⁷ where it is said that the study of a few excited states above the ground state is usually sufficient to explain most of the physical properties. When the whole system is considered, these excited states represent *collective modes*, rather than the motion of the individual particles (atoms and electrons). The crystallographic approach describes a system in terms of a time aver-

age of the individual atom motions. The collective modes of motion of a system of $\sim N_{av}$ atoms in a solid include the possible sound waves which propagate through the solid; when they are quantized, they exhibit particlelike behavior and act as weakly interacting quasiparticles called *phonons*. They represent, of course, an important component of the dielectric function. Since experiments are always performed at given temperature and wavelength, the problem will always consist in solving systems of truly *interacting* particles; that is, *diffraction is affected by the behaviors of the dielectric function*. The dielectric function, in fact, represents the bridge be-

tween the physical and crystallographic approaches because the behaviors of the first excited states are playing a major role in the features of this function. Therefore the Hamiltonian discussion which follows and the analysis of the dielectric function are interchangeable.

V. HYPOTHESIS FOR DESCRIBING THE PHYSICAL APPROACH

We stress that we restrict the discussion to the case of small vibrations for compounds where the square roots of the mean-square displacements represent a few percent of the dimensions of the unit cell (see Table II). This means that we only consider perturbative anharmonicity to explain the observed

data even though anharmonic contributions may increase the results given in the sixth column of Table II. In doing so, we justify power-series expansions of the potential energies. It is known that a general anharmonic model invalidates the superposition principle and that it has to be replaced by models such as those proposed by Matsumoto and Umezawa²⁸ or by DeFacio and Hammer.²⁹ Furthermore, $\chi(\omega, \vec{H})$ can contain coherent components from many unit cells. If \vec{x}_i is the vector indicating the position of the i th atom of mass m_i such as $\vec{x}_i = (x_{i1}, x_{i2}, x_{i3})$ where $x_{i\alpha}$ ($\alpha = 1, 2, 3$), then the measure of the displacements $\zeta_{i\alpha}$ for the i th atom along the α component from its equilibrium position is defined as $\zeta_{i\alpha} \equiv x_{i\alpha} - x_{i\alpha}^{(0)}$, where $\alpha = 1, 2, 3$.

VI. HAMILTONIANS AND ELECTRON-CHARGE DENSITY DISTRIBUTIONS

The kinetic energy of vibrations of all atoms in the solid is

$$K = \frac{1}{2} \sum_{i=1}^N \sum_{\alpha=1}^3 m_i \dot{x}_{i\alpha}^2 = \frac{1}{2} \sum_{i=1}^N \sum_{\alpha=1}^3 m_i \dot{\zeta}_{i\alpha}^2. \quad (17)$$

Since only small displacements from equilibrium are considered, the potential energy $V = V(x_{11}, x_{12}, x_{13}, x_{21}, \dots, x_{N3})$ can be expanded in Taylor's series:

$$\begin{aligned} V = V_0 + \sum_{i,\alpha} \left[\frac{\partial V}{\partial x_{i\alpha}} \right]_0 \zeta_{i\alpha} + \frac{1}{2} \sum_{i,\alpha} \left[\frac{\partial^2 V}{\partial x_{i\alpha} \partial x_{j\beta}} \right]_0 \zeta_{i\alpha} \zeta_{j\beta} + \frac{1}{6} \sum_{i,\alpha} \left[\frac{\partial^3 V}{\partial x_{i\alpha} \partial x_{j\beta} \partial x_{k\gamma}} \right]_0 \zeta_{i\alpha} \zeta_{j\beta} \zeta_{k\gamma} \\ + \frac{1}{24} \sum_{i,\alpha} \left[\frac{\partial^4 V}{\partial x_{i\alpha} \partial x_{j\beta} \partial x_{k\gamma} \partial x_{l\delta}} \right]_0 \zeta_{i\alpha} \zeta_{j\beta} \zeta_{k\gamma} \zeta_{l\delta} + \dots, \end{aligned} \quad (18)$$

where $i = j = k = l = 1$ to N and $\alpha = \beta = \gamma = \delta = 1, 2$, or 3 . V_0 is simply the potential energy in the equilibrium configuration of the atoms. That is, V_0 represents the potential energy given by the positions of the atoms in the unit cell. V_0 then contains the structure of a given arrangement of atoms within a proper space. The subscript zero on the partial derivatives means that the successive derivatives are evaluated at the equilibrium positions. For a stable solid, the potential energy must be a minimum, consequently $(\partial V / \partial x_{i\alpha})_0 = 0$, which implies that the forces acting on any atom must vanish. Therefore, the lattice Hamiltonian (or energy) H_L associated with the vibrations of the atoms in the solid has the form

$$H_L = K + V = \frac{1}{2} \sum_{i,\alpha} m_i \dot{\zeta}_{i\alpha}^2 + V_0 + \frac{1}{2} \sum_{i,\alpha} A_{i\alpha,j\beta} \zeta_{i\alpha} \zeta_{j\beta} + \frac{1}{6} \sum_{i,\alpha} A'_{i\alpha,j\beta,k\gamma} \zeta_{i\alpha} \zeta_{j\beta} \zeta_{k\gamma} + \frac{1}{24} \sum_{i,\alpha} A''_{i\alpha,j\beta,k\gamma,l\delta} \zeta_{i\alpha} \zeta_{j\beta} \zeta_{k\gamma} \zeta_{l\delta} + \dots, \quad (19)$$

where $A_{i\alpha,j\beta}$ is the dynamical matrix in the harmonic approximation, $A'_{i\alpha,j\beta,k\gamma}$ represents the dynamical matrix for the third-order anharmonicity, and $A''_{i\alpha,j\beta,k\gamma,l\delta}$ is the dynamical matrix for the fourth-order anharmonicity. The last three sums in the

above expression reflect the fact that the atoms do interact. That is, atoms in a solid do not behave like independent particles. An illustration of these last three terms is given by the nonzero slope observed for $V_3\text{Si}$ when the ratio of the structure factors at 80

and 300 K are plotted as a function of $(\sin\theta/\lambda)^2$.³⁰ This relatively simple experimental procedure shows that the harmonic approximation should be abandoned even though it always gives good least-squares reliability factors. They are a measure of the goodness of the fit. Once the hypothesis of small-amplitude vibrations is fulfilled—which is always the case for the materials listed in Table II—then good reliability factors will always be found with simple harmonic models. The crystallographic approach at the harmonic level does not contain any physics, it is purely geometrical since it is based on the superposition of free spherical atoms and symmetry. Furthermore, harmonic anisotropy least-squares treatment of small-amplitude vibrations will take care of very small deviations, which, as has been shown for V_3Si ,³⁰ represent not harmonic anisotropy but anharmonicity. On the other hand, difference ECD's do contain chemico-physical information directly related to the last three terms of Eq. (19) because the inverse Fourier transform involves the difference between the observed and the calculated structure factors, the chemico-physical content being part of the observed structure factors. As it was very well explained by Ashcroft and Mermin¹⁷ and on a somewhat different level by Daughton and DeFacio,³¹ one cannot stop the development of the potential energy in power series at an odd-power term (third, fifth, . . .). As an illustration, the analysis of V_3Si at 78 K has shown that the quartic term dominates the cubic one and that the nonzero slope, mentioned above, is mainly due to the quartic term alone (Ref. 30 and Table III). This example clearly shows the need for a more thorough analysis of any data even when the small vibrational amplitude assumption is a good one (see Table II).

The problem is not solved by only taking into ac-

count the above lattice Hamiltonian. It is *necessary* to include H_e , which represents the electron-electron interaction including correlation effects from electrons belonging to different atoms (the electron-electron interaction within an atom is, in principle, taken care of by the form factor; see Fig. 2), and H_{e-ph} , which represents the interaction between electrons and phonons. H_{e-ph} has expressions of at least comparable magnitude as the cubic or quartic anharmonicity and, in the case of superconductivity, it may qualitatively change the system. Therefore, if one includes anharmonic terms, it is necessary in principle to add H_{e-ph} . In the simplest cases it is the correlation between one electron and one phonon. The magnitude and the impact of such an effect on a difference ECD can be locally enormous. In this respect the analysis made for V_3Si at 78 K (Ref. 30 and Table III) is incomplete and more work is needed to gain a better understanding of the softening and the incipient instability and related electronic properties. Finally, the total Hamiltonian within the framework of the small-amplitude vibration hypothesis and the superposition principle can be expressed by a superposition of independent terms of the form

$$H = H_L + H_e + H_{e-ph} + \dots \quad (20)$$

When a Fourier transform is performed on the differences between the observed structure factors and the calculated ones, the results depend very strongly upon the model used to compute the calculated structure factors. On the assumption that the superposition principle is adequate to treat anharmonic vibrations, it follows that the computation of deformation ECD maps would be, in fact, a consequence of the following residual Hamiltonian H_R :

TABLE III. Comparison of the various atomic vibration amplitudes in V_3Si as a function of the temperature (Refs. 30, 33, and 70). The \sim sign means that an average has been made on the various components of the thermal parameters for the V atoms. The second line (per temperature) gives the thermal parameters for the Si atoms. For comparison they are all expressed in units of Å. This shows that the quartic contribution is large but that its fourth power is small enough for perturbative treatment (see text).

T (K)	Lattice constant (Å)	Harmonic	Anharmonic treatment		
		approx. alone (Å)	Quadratic (Å)	Cubic (Å)	Quartic (Å)
13.5	4.719	~ 0.0416	~ 0.0375	< 0.0215	0.0669
		0.0465	0.0595	none	0.0790
78	4.718	~ 0.0562	~ 0.0547	0.0276	0.0865
		0.0594	0.0643	none	0.0853
300	4.724	~ 0.0729	~ 0.0710	0.0311	0.0865
		0.0755	0.0772	none	0.1026

$$H_R = H_e + H_{e-ph} + \dots \quad (21)$$

When the harmonic approximation is employed in the computation of such maps then one has to add the contribution of $H_{L,anh}$ to the above residual Hamiltonian where $H_{L,anh}$ is the anharmonic part of the lattice Hamiltonian [see Eq. (19)] containing explicitly $A'_{i\alpha,j\beta,k\gamma}$ and $A''_{i\alpha,j\beta,k\gamma,l\delta}$. The fact that V_0 is absent in $H_{L,anh}$ [see Eq. (19)] is very important because it means that a deformation ECD map is only weakly structure dependent and can be mainly associated with and compared to physical properties. The weak dependence from the structure comes from the fact that Eq. (21) may contain structural effects. This means that almost identical deformation ECD maps for another structure should result in very similar physical properties. The fact that deformation ECD's are mainly related to physical properties is very well-illustrated by the three deformation ECD's published in Ref. 20 and also by the figures of this article. It also justifies, *a posteriori*, the usage of the various types of bonding in setting the starting points for the three main Debye classes.²⁰

Furthermore, the dynamics of the electronic orbitals have been, in principle, eliminated by the difference process. As already underlined, Eq. (20) is simpler to analyze than $\chi(\omega, \vec{H})$ within the postulated hypotheses because the various contributions to the ECD can in principle be identified and isolated. By and large, however, Eq. (20) is not as general as $\chi(\omega, \vec{H})$, and one has to be very careful with conclusions that can be drawn from it. In addition, one notes that since the bonding type depends on physical properties and only weakly upon the structure, the technique of comparing ECD's from one structure to another without considerations for the physical properties is a possible source of confusion.

The discussion of valence ECD is more complicated because the valence electrons have been retained in the difference process. They can be split into two different categories: Those located around the atomic positions and those showing delocalizations and bonds. The localized valence-electron orbitals have a distribution similar to the one of the core electrons and, therefore, strongly contribute to the enhancement of the densities near the atomic positions (see Figs. 6 and 8). The delocalized valence electrons responsible for bonding and/or physical properties should have the same ECD distribution as that of the ones exhibited by deformation ECD's. This means that the ECD contributions given by Eq. (21) should be the same in the valence ECD as well as in the deformation ECD. Therefore a valence ECD expresses the superposition of localized valence electrons and ECD contributions from Eq. (21). When deformation and valence ECD maps

tend to disagree, one can invoke the fact that the superposition of the localized valence electrons and ECD contributions from Eq. (21) represents a different spatial ECD than deformation ECD which is a representation of Eq. (21). When this discrepancy becomes important, chemists often employ the terminology of "diffuse orbitals." In other words, these diffuse orbitals add some relatively constant density on top of the localized valence-electron density. This means that compounds characterized by diffuse orbitals exhibit almost flat deformation ECD (see Cr₃Si), while others having well-characterized orbitals show deformation ECD with contrasted features (see V₃Si). This says that the electronic orbitals have a higher vibration amplitude in Cr₃Si than in V₃Si and that their time-averaged contribution to the ECD is spread over a larger volume than in the case of well-characterized orbitals. This is opposite to what would be expected if valence orbitals followed the thermal parameters of the cores. It further means that valence orbitals in V₃Si are in quasistatic configurations. That is, the valence-orbital motions are largely synchronized with the core vibrations. In this sense, the comparison between deformation and valence ECD's is extremely useful in pointing out sites where possible dynamical behaviors of electronic orbitals occur. As suggested by Bertaut the application of the superposition principle to bonds³² is not limited at all by the behavior of electronic orbitals and their thermal parameters represent a measurement of the vibration amplitude of the valence-electron orbitals.

VII. CHARGE INTEGRATION

Examinations of the published ECD's^{13,33,34} and Figs. 6—10 show that there is much less density at the Si sites than that at the V or Cr atomic positions. Free Si atoms have four valence electrons, V atoms have five, and Cr atoms have six. In the assumption of no charge transfer the density around the Si positions should be almost as important as that observed in the surroundings of the V atoms or the Cr atoms. From these observations one directly concludes that the Si atoms are giving electrons to the V atoms in V₃Si and to the Cr atoms in Cr₃Si. The issue becomes the assessment of the magnitude of the charge transfer from Si to either V or Cr in these two A15 alloys. "As plausible as it seems at the outset to assign a definite charge, we must realize that even if we knew precisely the charge distribution at all points in the crystal, there is no unique way to divide it up and associate different parts with different atoms. Thus there is no unique atomic charge."³⁵ Since ECD maps are usually computed

for planes orthogonal to one of the main crystallographic axes, the simplest volumes that can be centered around atoms and attributed to each of them are subvolumes of the unit cell: cube for cubic structures and so on. The first attempt to assess the charge transfer from Si to V has been made by integrating the total ECD within disconnected cubic boxes of identical volume attributed to each of these two atoms.³⁶ This method showed that -1.2 ± 0.4 electrons have been found on the Si atom compared with the neutral atom and $+0.4 \pm 0.2$ electrons for the V atoms.³⁶ If one assumes that the volume of the unit cell must be completely distributed among volumes attributed to atoms composing the unit cell, then this simple method can only furnish the lower limit of the charge transfer. On the other hand, if one wants to compare experimental integrations with results given by integrating theoretical charges according to the muffin-tin spheres method, then the experimental method described above should give a higher charge transfer than the ones computed by Klein *et al.*³⁷ In their Table V, Klein *et al.* give a charge of 21.2 electrons inside of the muffin-tin sphere for V, 12.3 electrons inside of the muffin-tin for Si, and 14.2 electrons outside of the two above muffin-tin spheres for V_3Si . One notes directly that the calculated charge on Si is intermediate between the results given in Ref. 13 and the ones published in Ref. 36. This is no surprise, because the ECD's are quite flat in the vicinity of Si atoms. The disagreement comes from the comparison for V atoms. Apparently the densities computed by the self-consistent augmented-plane-wave method have less structure than the densities determined experimentally. Although we understand some of the reasons why the band theorists choose the muffin-tin-sphere approximation, we believe that describing a two-atom system with three different volumes does not give a clear picture of the charge transfer within such a system. Therefore it is simpler to interpret a charge transfer when the volume of the unit cell is divided into the same number of volumes as the number of atoms composing it and when the volumes assigned to the atoms completely fill the volume of the unit cell. Thus, the generalization of the Wigner-Seitz cells seems (see Fig. 3) the best way to treat this problem.³⁸

From Fig. 4 we note that there are no significant differences between the integrations of the deformation ECD and the valence ECD for V_3Si .¹³ Furthermore, the integration on the total ECD also gives the same result.³⁹ For Cr_3Si ,³⁴ however, one immediately sees from Fig. 5 that there are significant differences between the integrations of the deformation and the valence ECD's. Unfortunately, for financial reasons, the integration of the total ECD

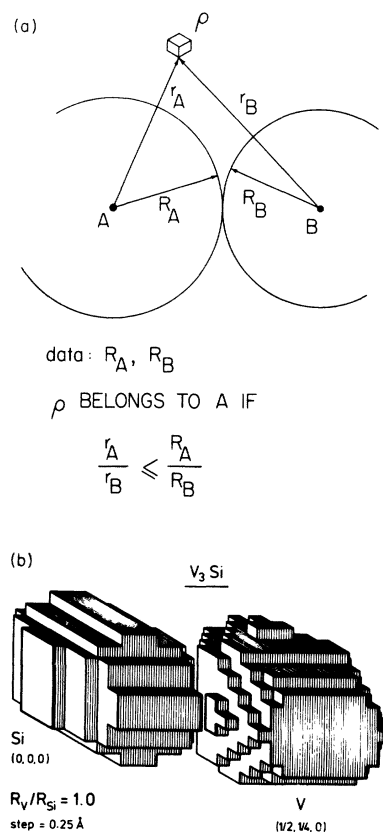


FIG. 3. (a) shows how a portion of ECD (usually a small subset of the unit cell) is attributed to the atom *A* or *B* depending on the ratio of the respective distances with respect to the ratio of the van der Waals radii. (b) Generalized Wigner-Seitz cells for V_3Si where $R_V/R_{Si}=1$ and corresponding to the first plateau of Fig. 4. These cells are similar to the one published in Ref. 13 and computed with the method described in Ref. 38(b).

has not been computed for Cr_3Si . Before explaining the reasons for such differences, we would like to point out some discrepancies between the results shown here in Fig. 4 and Fig. 1 of Ref. 13 on one hand and Fig. 5 of the present publication and Fig. 2 of Ref. 34 on the other hand. They are entirely concerned with the values on the axis representing R_A/R_{Si} where *A* is either V or Cr. Somehow and for reasons not yet fully understood, the computer program used in Refs. 13 and 34 shifted all R_A/R_{Si} positively by about 0.4. As a consequence of this shift, irrelevant digressions have been made about ionic radii in V_3Si (Ref. 13) and Cr_3Si .³⁴ The excellent agreement between the integrations in the three types of ECD for V_3Si on the one hand and the poor agreement for the two types of ECD in Cr_3Si on the other hand underline the point about the dynamics

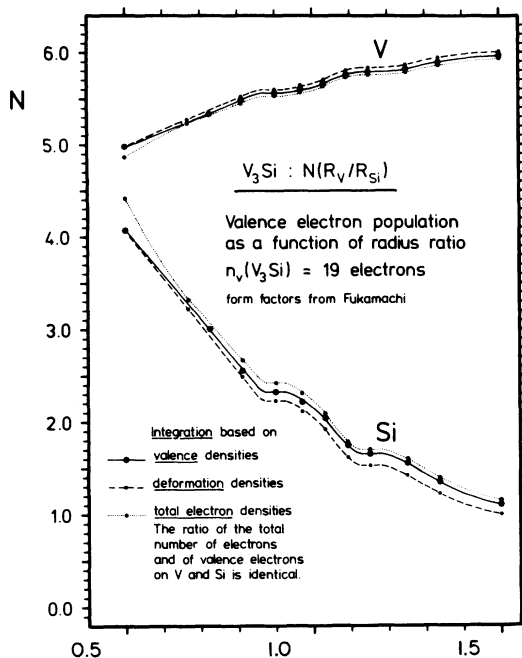


FIG. 4. Plot of the atomic charge integrations for the deformation, the valence, and the total ECD's in V_3Si according to the method reported in Ref. 38(b).

of the valence electrons orbitals made above (see Sec. VI). The integration of the deformation and valence ECD's is consequently very important in determining the possible dynamical effects for the valence-electron orbitals.

VIII. DESCRIPTION OF Cr_3Si AT ROOM TEMPERATURE

Figure 6 shows the valence ECD of Cr_3Si at room temperature and Fig. 7 exhibits the corresponding deformation density. By comparing these two maps, one sees that they are different despite earlier discussions³⁴ based solely on valence ECD for Cr_3Si . Our fundamental knowledge is now sufficient to explain these differences and replace supposed static situations by static and dynamical ones. The pileup of charges between two consecutive Cr atoms on a chain in Fig. 6 and the low density shown in Fig. 7 or the absence of charge²⁰ at the same point is a strong indication that a *dynamical* compression is occurring between relatively unperturbed valence-electron shells on a Cr chain in Cr_3Si . This compression is in good agreement with the ideas developed by Frank and Kasper⁴⁰ even though they were based on geometric (static) considerations. There are also some details along curved lines be-

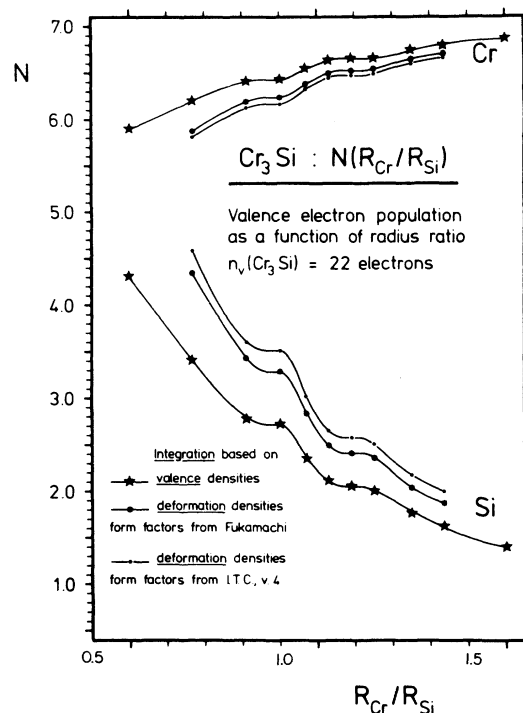


FIG. 5. Plot of the atomic charge integrations for the deformation and the valence ECD's in Cr_3Si according to the method reported in Ref. 38(b).

tween Si and Cr atoms which are apparent in Fig. 7 and nonexistent in Fig. 6 and the closest ones from the Cr sites could be attributed to consequences of Eq. (21). The pileups of charges around the Si atom are exaggerated in Fig. 6 as compared with their small counterparts in Fig. 7. This also indicates important dynamical contributions from the part of the Si valence electrons which are not perturbed by the bonding.

IX. DESCRIPTION OF V_3Si AT 300 AND 13.5 K

The crystal of V_3Si studied was a transforming one. We already mentioned the difficulties in refining the crystallographic parameters.^{30,33} Although we did not properly treat the static displacements,⁷ we showed that below the martensitic transition the cubic approximation gave a better fit than any attempted noncubic groups (see Table IV).

After measuring the (111), (300), (003), (110), (101), (200), and (002) reflections in Nb_3Sn at 33 K and the (300) reflection as a function of the temperature below the martensitic transition temperature (~ 45 K), Shirane and Axe⁴¹ concluded that the

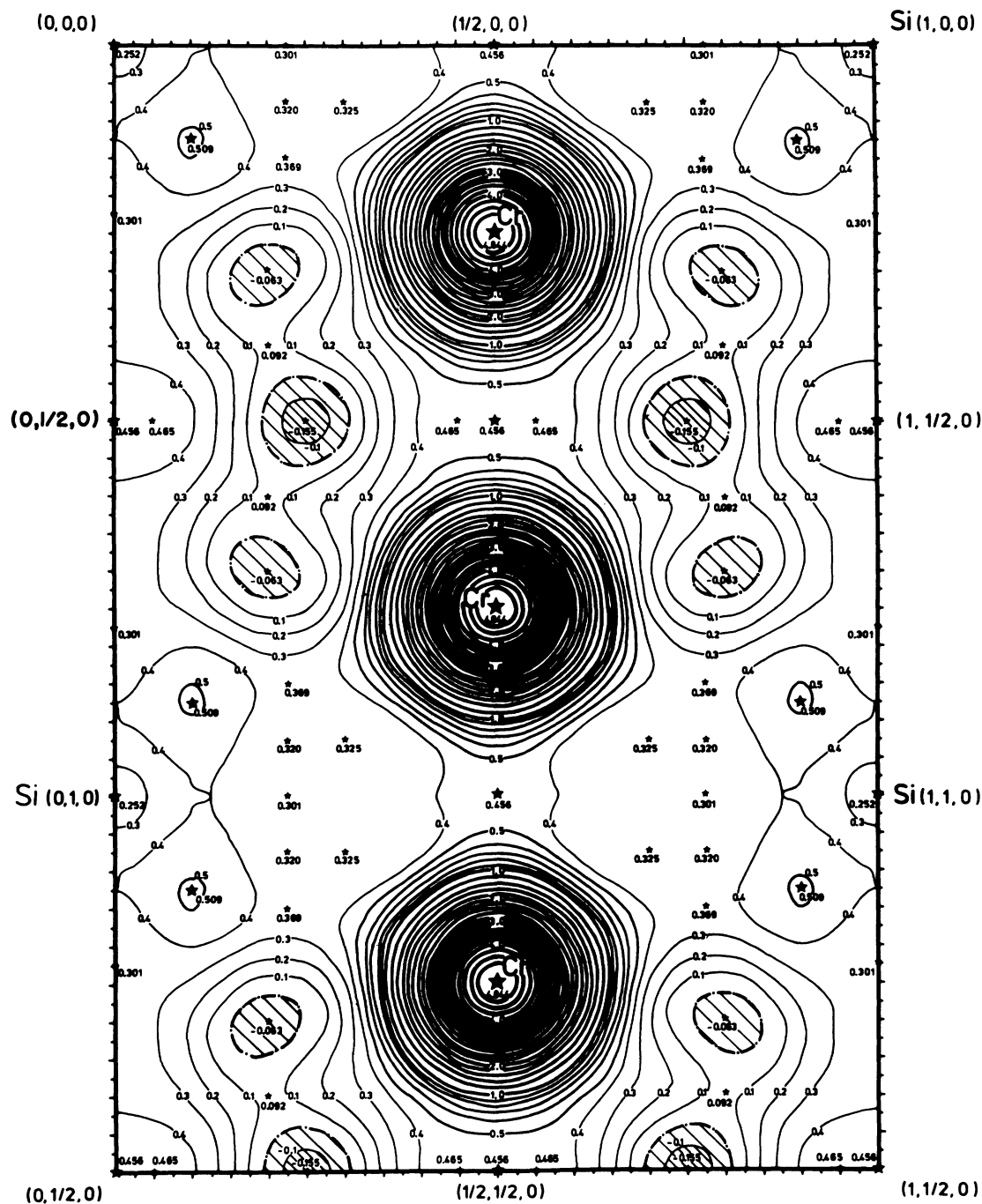


FIG. 6. Valence-electron charge density map of Cr_3Si at 300 K in the (001) plane according to Ref. 34. It shows one and a half faces of the unit cell in order to better illustrate the shape of the ECD contours around a Cr chain. Contours at $0.1 e \text{ \AA}^{-3}$ interval below the $1.0 e \text{ \AA}^{-3}$ level and at $0.2 e \text{ \AA}^{-3}$ interval above the $1.0 e \text{ \AA}^{-3}$ level. Negative densities are shaded. Reflections up to $\sin\theta/\lambda = 0.6 \text{ \AA}^{-1}$ are included in the inverse Fourier transform.

space group for the low-temperature structure of Nb_3Sn is $P4_2/mmc$. From the literature it appears that some physicists hold that the low-temperature structure of V_3Si is the same as that of Nb_3Sn (Ref.

42) while others doubt but still use this structure.⁴³ Table IV presents the various models considered in attempting to determine the true structure of V_3Si below the martensitic transition. Our results estab-

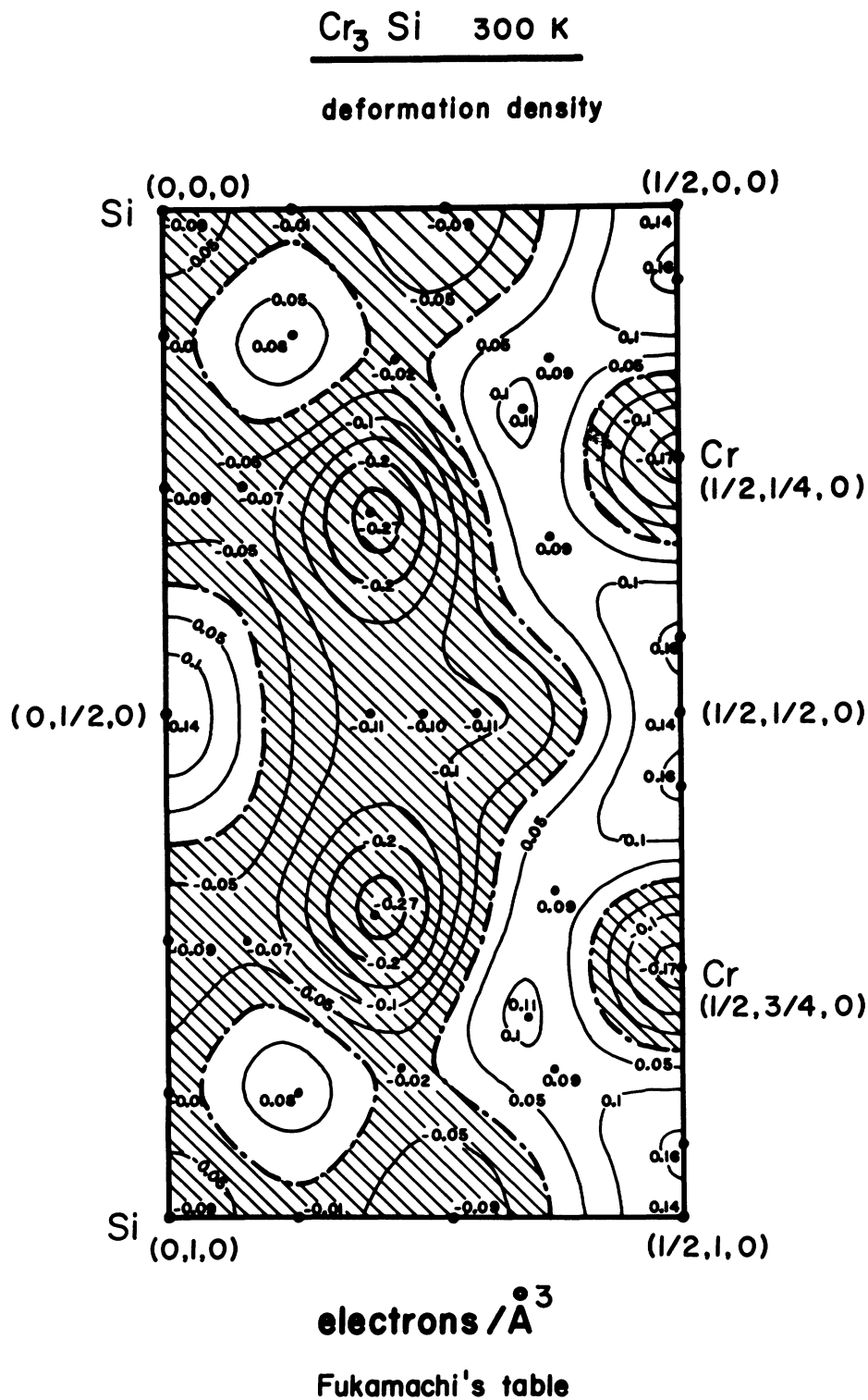


FIG. 7. Deformation electron charge density map of Cr₃Si at 300 K of half of a face unit in the (001) plane according to Ref. 20. Contours at 0.05 e Å⁻³ interval. Negative densities are shaded. Reflections up to $\sin\theta/\lambda=0.6 \text{ \AA}^{-1}$ are included in the inverse Fourier transform.

TABLE IV. Least-squares (LS) refinements made on the 13.5-K data in order to attempt the determination of the real martensitic structure of our transforming V_3Si crystal. The agreement factors $R(F)$ and $WR(F)$ are defined as follows: $R(F) = [\sum_{\vec{H}} (F_{obs} - F_{calc})^2 / \sum_{\vec{H}} F_{obs}^2]^{1/2}$, and $WR(F) = [\sum_{\vec{H}} W(F_{obs} - F_{calc})^2 / \sum_{\vec{H}} WF_{obs}^2]^{1/2}$, where W is the weight attributed to a structure factor $F(\omega, \vec{H})$. ITC 1 means *International Tables for X-ray Crystallography*, Vol. 1 (see Ref. 10).

Type of average made on observed equivalent structure factors (global symmetry)	Space group used in the LS process	Independent atoms and crystallographic positions from ITC 1	Number of independent reflections included in the least-squares process	Agreement factors $R(F)$ $WR(F)$		
Cubic	$Pm\ 3n$	V (6c)	155	0.0091		
		Si (2a)		0.0078		
Tetragonal	$Pm\ 3n$	V (6c)	400	0.0253		
		Si (2a)		0.0308		
		$P4_2/mmc$		V ₁ (4m)	432	0.0326
		V ₂ (2e)		0.0308		
	$P4_2mc$	V ₁ (4j)	432	0.0324		
		V ₂ (2a)		0.0306		
		Si (2c)				
		$P4_2/m$		V ₁ (4j)	432	0.0324
	$P4_2/m$	V ₂ (2e)	432	0.0305		
		Si (2d)				
		$P4_2$		V ₁ (4d)	432	0.0324
		V ₂ (2a)		0.0304		
Orthorhombic	$Pmmm$	Si (2c)	600			
		V ₁ (2r)		0.0329		
		V ₂ (2o)		0.0354		
		V ₃ (2j)				
		Si ₁ (1h)				
		Si ₂ (1a)				
	$Pmm\ 2$	V ₁ (2h)	600	0.0328		
		V ₂ (2f)		0.0353		
		V ₃ (2e)				
		Si ₁ (1d)				
		Si ₂ (1a)				

lish that the low-temperature structure of V_3Si is probably not the same as that of Nb_3Sn below the martensitic transformation. Beside the cubic approximation every case listed in Table IV presented major problems in refining the thermal parameter of the Si atom in the anisotropic form even when the chosen space group provides this possibility. The allowed general positions for the V atoms also introduced many difficulties into the refinements and very seldom showed any significant displacement from the cubic position. Based on the present data, the structure of V_3Si below the martensitic transition remains uncertain and, for the time being, the

best approximation is still the cubic $A15$ structure (see Table IV). Table 1 of Ref. 33 shows that the real structure could be as complicated as monoclinic in relative agreement with the work of Ullrich *et al.*⁴⁴ on plastically deformed V_3Si single crystals.

In contrast to the Cr_3Si ECD's at room temperature, the comparison of Figs. 8 and 9 and the results of the charge integrations (see Fig. 4) for V_3Si at 300 K show that the situation is fairly static, except perhaps, the Si delocalized valence electrons at $(\sim \frac{1}{4}, 0, 0)$ and symmetry related locations. The small difference ECD enhancement at $(\sim \frac{1}{4}, \frac{1}{4}, 0)$ has no valence ECD equivalent. This could perhaps

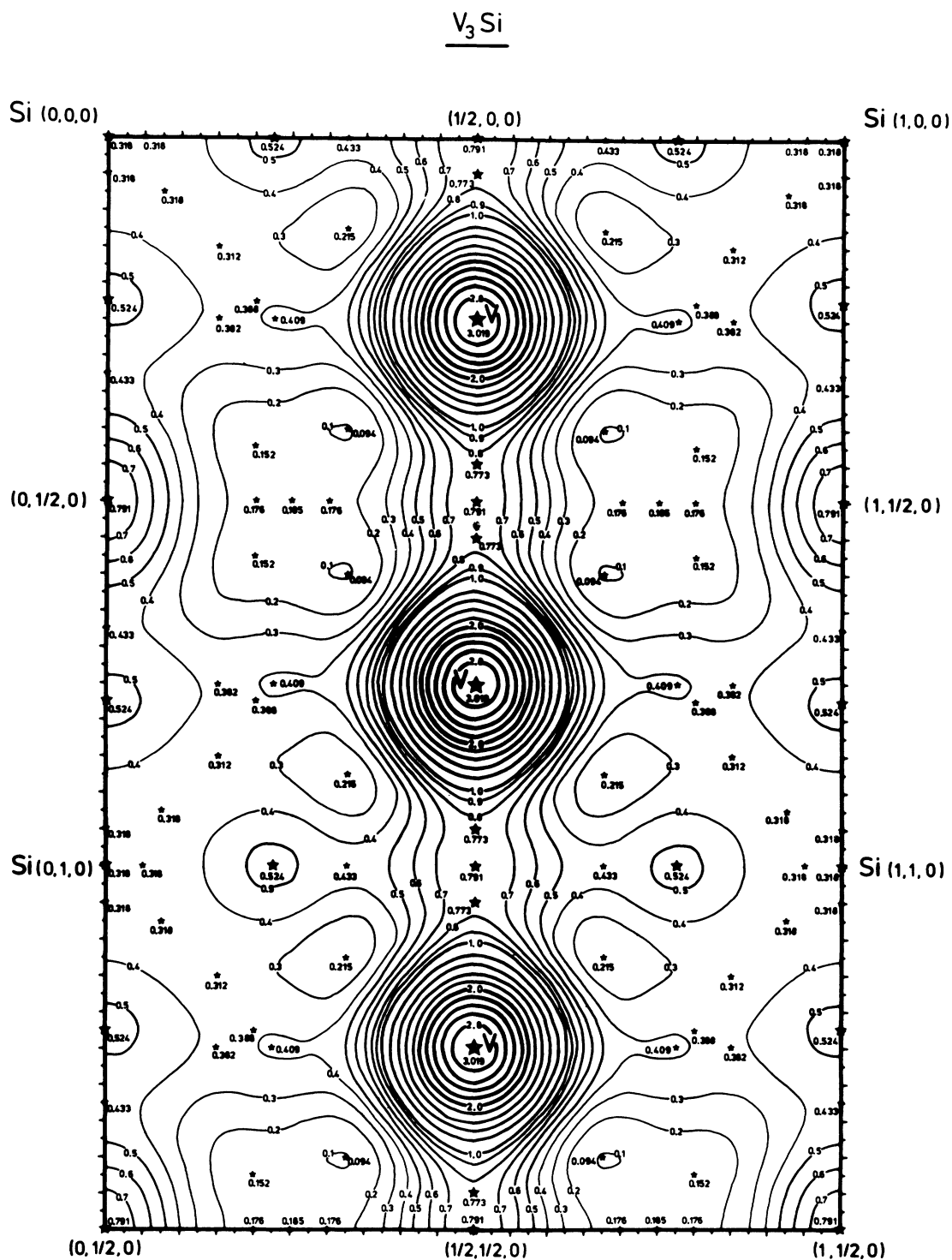


FIG. 8. Valence-electron charge density map for V_3Si at 300 K in the (001) plane according to Refs. 13 and 33. It shows one and a half faces of the unit cell in order to better illustrate the shape of the ECD contours around a V chain. Contours at 0.1 e \AA^{-3} interval below the 1.0 e \AA^{-3} level and at 0.2 e \AA^{-3} interval above the 1.0 e \AA^{-3} level. Negative densities are shaded. Reflections up to $\sin\theta/\lambda = 0.6 \text{ \AA}^{-1}$ are included in the inverse Fourier transform.

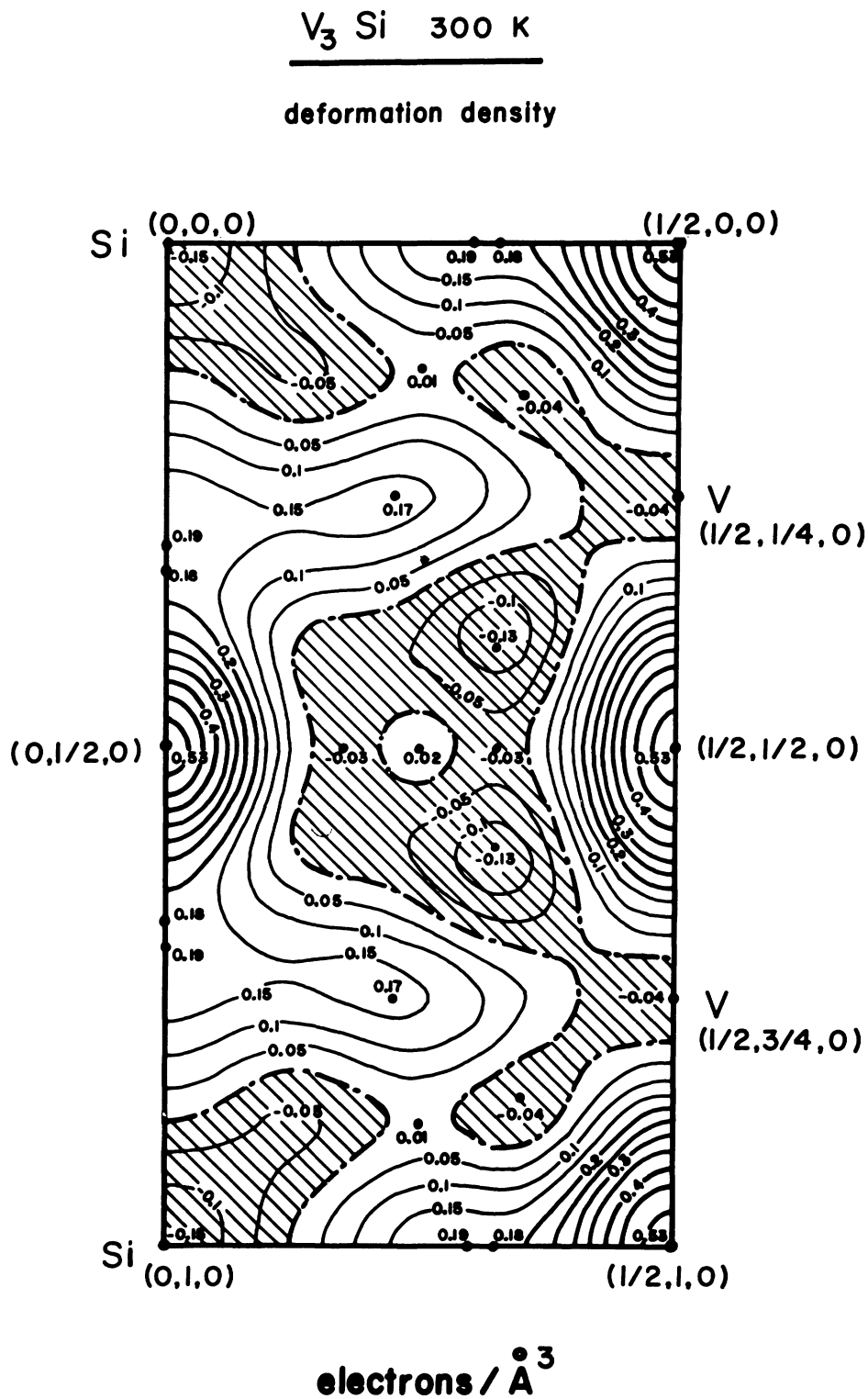


FIG. 9. Deformation electron charge density map for V_3Si at 300 K of half of a face unit in the (001) plane according to Refs. 13 and 20. Contours at $0.05 e/\text{\AA}^3$ interval. Negative densities are shaded. Reflections up to $\sin\theta/\lambda=0.6 \text{\AA}^{-1}$ are included in the inverse Fourier transform.

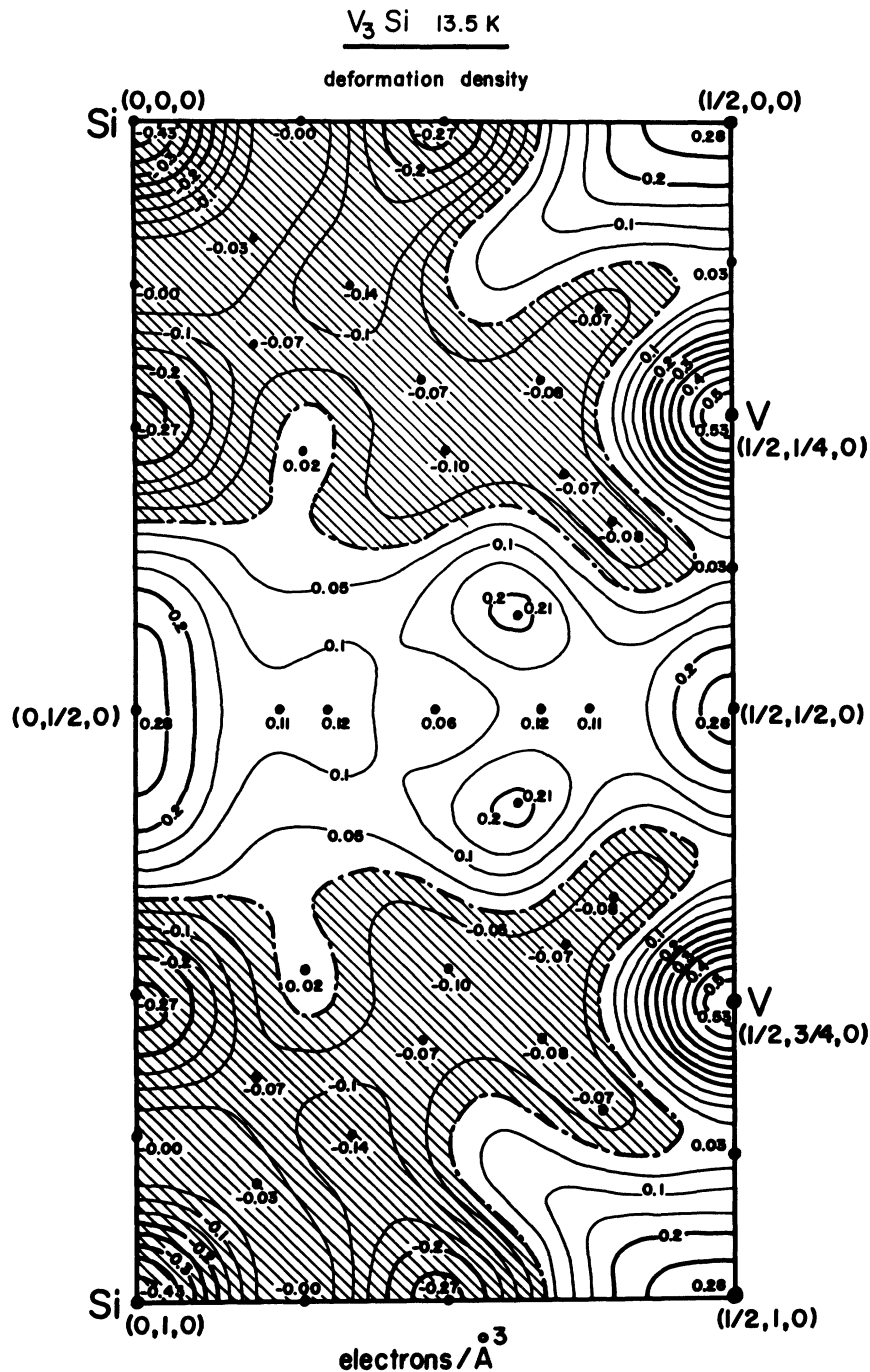


FIG. 10. Deformation electron charge density map for V_3Si of half of a face unit in the superconducting state (13.5 K) and in the (001) plane. This temperature is below both the superconducting transition (17 K) and the martensitic transformation (~ 22 K). Its corresponding valence electron charge density map is Fig. 2 of Ref. 33. Contours at 0.05 interval. Negative densities are shaded. Reflections up to $\sin\theta/\lambda = 0.65 \text{ \AA}^{-1}$ are included in the inverse Fourier transform.

be explained by a correlation contributions from Eq. (21).

As far as the differences between the ECD's at 300 and 13.5 K are concerned, Figs. 9 and 10 show that the biggest difference between the two maps is

that the pileup at $(\sim \frac{1}{4}, 0, 0)$ between the Si atoms and the V-V bonds on chains does not exist at 13.5 K (Fig. 10). There seems to be slightly more density at $(\sim \frac{1}{4}, \sim \frac{1}{2}, 0)$ between two perpendicular chains at 13.5 K than at 300 K. Since this density enhance-

ment is well within the standard deviations (see Table I) there is, consequently, no clear evidence for electronic interaction between two perpendicular chains, in contradiction to some theoretical results^{45,46} but in qualitative agreement with more recent theoretical works.^{15,16,47} Mattheiss and Werner⁴⁷ explain the role of the Γ_{12} subbands as being the consequence of a strong interchain coupling and representing $\sim 3\%$ of the valence electrons. There are twelve equivalent $\sim(\frac{1}{4}, \frac{1}{2}, 0)$ positions in an $A15$ unit cell. Therefore the integration of the Γ_{12} subbands per $\sim(\frac{1}{4}, \frac{1}{2}, 0)$ point represents $\sim 0.25\%$ of the valence electrons which would give an experimentally detectable charge density. The experimental charge density at $\sim(\frac{1}{4}, \frac{1}{2}, 0)$ seems to say two things: (a) Mattheiss and Werner overestimated the electronic population of the Γ_{12} sub-

bands or (b) the way different chains are coupled to each other is more complicated than explained above and, therefore, experimental ECD cannot prove or disprove the Mattheiss and Werner result⁴⁷ about the Γ_{12} subbands.

The absence of charge density at $(\sim\frac{1}{4}, 0, 0)$ in the superconducting state shows that the V atom chains behave more independently below the martensitic transition than at room temperature. The deformation ECD (Fig. 10) exhibits peculiar significant protruberances around the V-V interaction and, of course, around the V atoms in the same chain. These deformations surround the V-V bond as two rings and can be seen more easily in Fig. 11. These rings do not exist at 300 K (see Fig. 9) and could be related to the disappearance of the electron interaction between Si atoms and V-V bonds on chains.

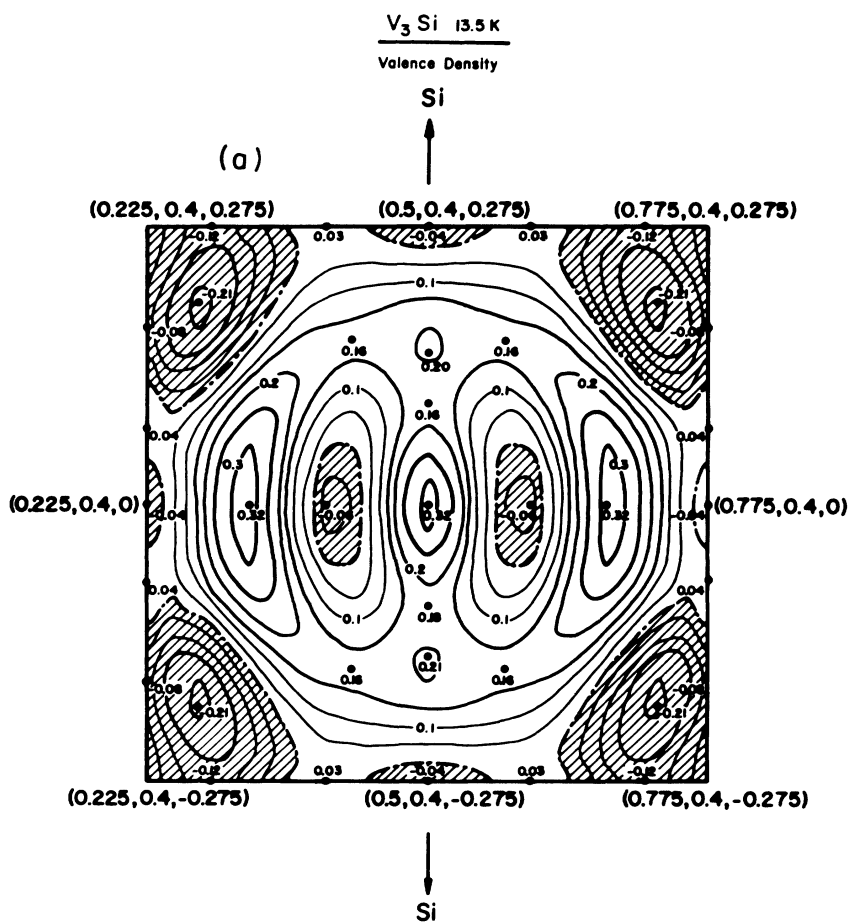


FIG. 11. Valence (a) and deformation (b) electron-charge-density maps of V_3Si in the superconducting state (13.5 K) showing the structure of the "rings" discussed in Fig. 10 and in Ref. 33 (see text). Contours at $0.05 e \text{ \AA}^{-3}$ interval. Negative densities are shaded. Reflections up to $\sin\theta/\lambda = 0.65 \text{ \AA}^{-1}$ are included in the inverse Fourier transform. The arrows pointed toward the Si indications show the direction of the closest Si atoms from this ring structure.

the coupling of the electron-phonon interaction⁵⁰ and the superconductivity in V_3Si . More theoretical insights are needed to understand this coupling as well as the effects of the dielectric function.²³ On the basis of remarks relating Nb_3Sn to V_3Si made in Ref. 20, the ring anisotropy in Nb_3Sn could be such that the electron density maximum is pointed toward Sn atoms rather than toward another chain as in V_3Si . This, of course, implies different structures for these two compounds below their respective martensitic transition. Because of the magnitude of the standard deviations on the densities (Table I) together with the magnitude of the distortion of the unit cell, the shape of these rings will not be significantly changed if the inverse Fourier transform is done with the true structure of the martensitic phase of V_3Si .

X. CONCLUSIONS

The end of Sec. VII (charge integration) contains a striking conclusion, showing that compounds having no significant dynamical contributions from the valence-electron orbitals are simpler to analyze and, at the same time, seem to exhibit enormous variations in their physical properties (see Ref. 6 for V_3Si as an example).

It is easy to see that the problem of determining whether a metal or an alloy has valence-electron orbitals with no significant dynamical contributions requires a sort of self-consistent procedure. The full evaluation of its ECD's (deformation and valence) as well as a complete charge integration procedure must be completed. The results are then checked to see whether $K_{val} \sim 0$. When it is, the present analysis shows that valence and deformation ECD's can be used interchangeably and that the valence-electron orbitals are in quasistatic configurations. It further implies that these compounds can be unstable and can lead to a rich collection of possible effects lowering the energy such as martensitic, superconducting, Jahn-Teller, or Peierls transitions. When $K_{val} \neq 0$, the valence ECD's still play an important role because a detailed comparison of the two ECD's allows to distinguish which density in the unit cell exhibits valence-electron orbitals with dynamical effects. It also means that electronic orbitals are almost in a free-particle-like eigenstate with a large positive energy.

Although our primary goal is a better understanding of the fundamental electronic contributions that are exhibited in ECD maps, it is worthwhile at this point to review our acquisitions about V_3Si and confront them with works from others. By comparing the x-ray diffraction data at 300 and 13.5 K, it can be seen that interactions in V_3Si are temperature

dependent and this cannot be explained without invoking Eq. (21). The same behavior is expected for Nb_3Sn .²⁰ We also noted that the V-atom chains are weakly bonded to the body-centered lattice of Si atoms. Therefore, the linear character of the V atom chains is a good approximation if ionic forces between the V and Si atoms are not taken into account (see below). This could partially explain the successes of simple models.⁴⁵⁻⁴⁹ From the work of Schweiss *et al.*⁵¹ on inelastic neutron scattering one can read that vibrational spectra in V_3Si is largely determined by the forces between the V and Si components. This conclusion is relatively temperature independent and valuable for other *A15* alloys. Since there is no pileup of charges along lines joining V and Si atoms at 13.5 K as well as at 300 K and since the density (that is the strength) of the bonds between Si atoms and V-V bonds on chains decreases below ~ 130 K (see Fig. 1), it is necessary to introduce important ionic electrostatic forces between the Si and V atoms in order to be in agreement with conclusions derived from inelastic neutron scattering on polycrystalline V_3Si .⁵¹ The large charge transfer found in V_3Si seems to support this conclusion (see Fig. 4 and Ref. 13). Therefore, ionic forces seem to be a temperature-independent feature of V_3Si and probably of most of the *A15* compounds. The comparison between the neutron scattering study of the dynamics of the lattice-phase transition in V_3Si by Shirane *et al.*⁵² and our work seems to show that the martensitic phase transition has probably an electronic origin—perhaps due to the disappearance of the pileup of charges between the Si atoms and the V-V bonds on chains—rather than originating from a softening of an optic phonon branch near the Brillouin-zone (BZ) center. Consequently, the pronounced softening in the elastic constants measured by Testardi and Bateman⁶ could also result from an electronic origin. Batterman and Barrett⁵³ described the observed transformation in V_3Si at ~ 21 K as a martensitic transition because it involves no diffusion. Anderson and Blount⁵⁴ pointed out that if the martensitic transition in V_3Si is a second-order transformation, this transition must depend on something else than strain. Because no superstructure and no magnetic anomaly were found in V_3Si , Anderson and Blount⁵⁴ have written: "We are left with two possibilities: (1) some electronic mystery parameter, associated perhaps with pairing; or (2) some change in symmetry, such as the loss of the inversion center, which cannot easily be observed with X-rays."⁵⁴ It is tempting to bring the possibility (1) of Anderson and Blount together with the pair of anisotropic rings found around each V-V bond in a chain in the 13.5 K measurement. Their second possibility could ei-

ther be another source of the martensitic transition or a consequence of the first possibility (anisotropic rings). For more details about the phase transition observed in some *A*15 compounds, one can consult the excellent article of Testardi⁵⁵ and the review of Lüthi and Rehwald.⁵⁶

Harrison³⁵ pointed out in his book the importance of the electronic arrangement on the dielectric function through the so-called "local-field corrections." These corrections arise because "the field at any one bond is affected by the polarization of any neighboring bond." Furthermore, Harrison continued by writing that: "Local field corrections may reduce the static dielectric constant by the order of 10%." This means that the more anisotropic an ECD is, the more pronounced is the effect on the dielectric function. Figures 6 and 8 clearly show that the anisotropy is not only more pronounced but also more extended around the atoms in V_3Si than it is around the atoms in Cr_3Si (see also Ref. 20). "Any increase in the dielectric constant of the medium, even if in only a part of it (the sources of the field remaining unchanged), reduces the total free energy."²⁴ This citation seems to contradict the local-field corrections one,³⁵ but any of these corrections implies a frequency renormalization (softening) such that the total free energy of the system is still a minimum. Consequently, the local-field corrections for the *A*15 compounds seems most pronounced when the anharmonicity is maximum, which, according to Eqs. (13) and (14), locally enhances the ECD. This local enhancement derives from the fact that the dielectric function depends upon the frequency and the reciprocal vector. These considerations explain why the charge transfer described in Sec. VII is significantly higher for V_3Si than for Cr_3Si . In a subsequent paper,²³ we plan to show more rigorously which are the most favorable experimental conditions for extracting local combination of the electron-electron and electron-phonon interactions.

A further consequence of this discussion is the danger in assigning electronic orbitals and decomposing them by the method of multipole decomposition.⁵⁷ It is now clear that this practice can only be done if the dynamical effects have been properly accounted for. Otherwise physical effects may be inadvertently treated as static electronic orbitals. In addition, the multipole scheme is strictly limited to cases where the orbitals are in quasistatic configuration (see Sec. VI).

Finally, the fact that $\rho(\omega, \vec{r})$ and $F(\omega, \vec{H})$ have an

explicit frequency (time) dependence has important practical consequences: (a) Competition between anisotropic extinction corrections and the anisotropy of the dielectric function. (b) Fourier transforming the various forms of independent reflections (especially at low \vec{H}) gives information about the anisotropy of the dielectric function and not, as is usually thought, about the anisotropy of the extinction. (c) The first few reflections (lowest values of \vec{H} or h, k, l) cannot in principle suffice to determine the extinction parameters because of the information about the dielectric function which they contain. Thus, the extinction parameters must be determined from the core electrons, together with the thermal parameters. This varies from standard crystallographic practice, as well as from the practice previously followed by one of us (J.-L.S.). Isotropic extinction corrections based on valence reflections (see Fig. 2) do not correct anisotropic features of the dielectric function, they simply rescale the ECD distribution.

The experimental determination of difference ECD's is a very important tool in the study of any phase transitions. It promotes the concept of the dynamics of the valence-electron orbitals. Consequently, precise ECD measurements are particularly useful to understand the dynamics of electronically driven phase transitions. In this respect, this method may become complementary to inelastic neutron scattering techniques. When our knowledge of ECD's improves, we should be able to predict locations of inelastic neutron peaks in the reciprocal space.

ACKNOWLEDGMENTS

One of us (J.-L.S.) thanks Dr. C. A. Swenson for assigning him the teaching duty of the course "Thermal Physics" where most of the present article emerged and evolved in the process of explaining to students the interactions between atoms. Dr. D. L. Cowan and Dr. R. Fuchs are gratefully acknowledged for their fundamental comments about the dynamics of the valence electron orbitals. We are indebted to Dr. J. C. Corbett for a thoughtful reading of the manuscript and to Dr. J. B. Cohen for useful remarks about orbitals. Ames Laboratory is operated for the U. S. Department of Energy by Iowa State University under Contract No. W-7405-Eng-82. This work was supported by the Director for Energy Research, Office of Materials Science Division.

- ¹L. Auslander and R. Tolimieri, *Bull. Am. Math. Soc.* **1**, 847 (1979).
- ²G. W. Mackey, *Bull. Am. Math. Soc.* **3**, 543 (1980).
- ³P. Coppens, in *Neutron Diffraction*, edited by H. Dachs (Springer, Berlin, 1978), pp. 71–111.
- ⁴T. H. K. Barron, A. J. Leadbetter, J. A. Morrison, and L. S. Salter, *Acta Crystallogr.* **20**, 125 (1966).
- ⁵P. Flubacher, A. J. Leadbetter, and J. A. Morrison, *Philos. Mag.* **4**, 273 (1959).
- ⁶J. R. Testardi and T. B. Bateman, *Phys. Rev.* **154**, 402 (1967).
- ⁷J.-L. Staudenmann, B. DeFacio, and L. R. Testardi (unpublished).
- ⁸R. Hosemann and S. N. Bagchi, *Direct Analysis of Diffraction by Matter* (North-Holland, Amsterdam, 1962). Citations start at p. 120 and at p. 463.
- ⁹T. Fukamachi, Technical Report of ISSP, Series B 12, the Institute for Solid State Physics, The University of Tokyo, Roppongi, Minato-ku, Tokyo, 1971 (unpublished).
- ¹⁰*International Tables for X-ray Crystallography* (Kynoch, Birmingham, 1974), Vol. 4.
- ¹¹(a) P. J. Brown, *Philos. Mag.* **26**, 1377 (1972); (b) R. F. Stewart, *Acta Crystallogr. Sect. A* **33**, 33 (1977); (c) Y. W. Yang and P. Coppens, *ibid.* **34**, 61 (1978); (d) D. M. Collins and F. W. Whitehurst, *ibid.* **37**, 848 (1981).
- ¹²B. Rees, *Acta Crystallogr. Sect. A* **32**, 483 (1976); Israel J. Chem. **16**, 180 (1977).
- ¹³J.-L. Staudenmann, P. Coppens, and J. Muller, *Solid State Commun.* **19**, 29 (1976).
- ¹⁴K.-M. Ho (unpublished results).
- ¹⁵L. F. Mattheiss and D. R. Hamann, *Solid State Commun.* **38**, 689 (1981).
- ¹⁶P. K. Lam and M. L. Cohen, *Phys. Rev. B* **23**, 6371 (1981).
- ¹⁷N. W. Ashcroft and N. D. Mermin, *Solid State Physics* (Holt, Rinehart and Winston, New York, 1976), particularly Chap. 25.
- ¹⁸O. Madelung, *Introduction to Solid State Theory* (Springer, Berlin, 1978).
- ¹⁹G. D. Mahan, *Many Particle Physics* (Plenum, New York, 1981).
- ²⁰J.-L. Staudenmann, B. DeFacio, L. R. Testardi, S. A. Werner, R. Flukiger, and J. Muller, *Phys. Rev. B* **24**, 6446 (1981).
- ²¹R. W. James, in *Solid State Physics*, edited by F. Seitz and D. Turnbull (Academic, New York, 1963), Vol. 15, pp. 53–220.
- ²²B. W. Batterman and H. Cole, *Rev. Mod. Phys.* **36**, 681 (1964).
- ²³B. DeFacio and J.-L. Staudenmann (unpublished).
- ²⁴L. D. Landau and E. M. Lifshitz, *Electrodynamics of Continuous Media* (Pergamon, Oxford, 1975). See especially pp. 58–64 and observe that this discussion is incomplete since the final relation between the divergence of a local electric field and the structure factor is not given. See also Chap. 9.
- ²⁵A. M. Colgston and V. Jaccarino, *Phys. Rev.* **121**, 1357 (1961), and references therein for the experimental work; A. M. Colgston, A. C. Gossard, V. Jaccarino, and Y. Yafet, *Rev. Mod. Phys.* **36**, 170 (1964); D. I. Bardos, R. M. Waterstrat, T. J. Rowland, and J. B. Darby, *J. Low Temp. Phys.* **3**, 509 (1970); F. J. Fradin and J. D. Williamson, *Phys. Rev. B* **10**, 2803 (1974).
- ²⁶A. Treyvaud (private communication).
- ²⁷F. Reif, *Fundamentals of Statistical and Thermal Physics* (McGraw-Hill, New York, 1965), particularly Chap. 10.
- ²⁸H. Matsumoto and H. Umezawa, *Fortschr. Phys.* **24**, 357 (1976).
- ²⁹B. DeFacio and C. L. Hammer, *J. Math. Phys.* **17**, 267 (1976).
- ³⁰J.-L. Staudenmann and L. R. Testardi, *Phys. Rev. Lett.* **43**, 40 (1979); **44**, 553 (1980); *d- and f-band Metals*, edited by H. Shull and M. B. Maple (Academic, New York, 1980), pp. 247–257.
- ³¹W. J. Daughton and B. DeFacio, *J. Phys. C* **11**, 4307 (1978).
- ³²E. F. Bertaut, private communication and *J. Phys. (Paris)* **39**, 1331 (1978).
- ³³J.-L. Staudenmann, *Solid State Commun.* **26**, 461 (1978).
- ³⁴J.-L. Staudenmann, *Solid State Commun.* **23**, 121 (1977).
- ³⁵W. A. Harrison, *Electronic Structure and the Properties of Solids (The Physics of the Chemical Bond)* (W. H. Freeman, San Francisco, 1980), and important references therein; citations are from p. 97 and p. 124.
- ³⁶J.-L. Staudenmann, *Helv. Phys. Acta* **47**, 39 (1974).
- ³⁷B. M. Klein, L. L. Boyer, D. A. Papaconstantopoulos, and L. F. Mattheiss, *Phys. Rev. B* **18**, 6411 (1978).
- ³⁸(a) R. M. Moon, *Int. J. Magn.* **1**, 219 (1971); (b) P. Coppens, *Phys. Rev. Lett.* **35**, 98 (1975); (c) F. L. Hirshfeld, *Israel J. Phys.* **16**, 198 (1977).
- ³⁹J.-L. Staudenmann, thesis, University of Geneva, 1976 (unpublished).
- ⁴⁰F. C. Frank and J. F. Kasper, *Acta Crystallogr.* **11**, 184 (1958); **12**, 483 (1959).
- ⁴¹G. Shirane and J. D. Axe, *Phys. Rev. B* **4**, 2957 (1971); J. D. Axe and G. Shirane, *ibid.* **8**, 1965 (1973); G. Shirane, *Rev. Mod. Phys.* **46**, 437 (1974).
- ⁴²J. Labbé, *Phys. Rev.* **172**, 451 (1968) (see also Ref. 48).
- ⁴³J. Wanasele and B. W. Batterman, *J. Appl. Phys.* **41**, 3610 (1971).
- ⁴⁴H.-J. Ullrich, U. Reinhold, S. Daebritz, P. Paufler, K. Kleinstueck, and B. Pietrass, *Phys. Status Solidi A* **49**, 323 (1978).
- ⁴⁵L. F. Mattheiss, *Phys. Rev. B* **12**, 2161 (1975).
- ⁴⁶M. Weger and I. B. Goldberg, *Solid State Physics*, edited by H. Ehrenreich, F. Seitz, and D. Turnbull (Academic, New York, 1973), Vol. 28; I. B. Goldberg, *J. Phys. C* **8**, 1159 (1975).
- ⁴⁷L. F. Mattheiss and W. Weber, *Phys. Rev. B* **25**, 2248 (1982); private communication.
- ⁴⁸J. Labbé and J. Friedel, *J. Phys. (Paris)* **27**, 153 (1966); **27**, 303 (1966).

- ⁴⁹R. W. Cohen, G. D. Cody, and J. J. Halloran, *Phys. Rev. Lett.* **19**, 840 (1967).
- ⁵⁰G. Grimvall, *Phys. Scr.* **14**, 63 (1976), and references therein; G. B. Arnold, J. Zasadzinski, J. W. Osmun, and E. L. Wolf, *J. Low Temp. Phys.* **40**, 225 (1980); E. L. Wolf, J. Zasadzinski, G. B. Arnold, D. F. Moore, J. M. Rowell, and M. R. Beasley, *Phys. Rev. B* **22**, 1214 (1980); E. L. Wolf, D. M. Burnell, Z. G. Khim, and R. J. Noer, *J. Low Temp. Phys.* **44**, 89 (1981).
- ⁵¹B. P. Schweiss, B. Renker, E. Schneider, and W. Reichardt, in *Superconductivity in d- and f-Band Metals*, edited by D. M. Douglass (Plenum, New York, 1976).
- ⁵²G. Shirane, J. D. Axe, and R. J. Birgeneau, *Solid State Commun.* **9**, 397 (1971).
- ⁵³B. W. Batterman and C. S. Barrett, *Phys. Rev. Lett.* **13**, 390 (1964); *Phys. Rev.* **145**, 296 (1966).
- ⁵⁴P. W. Anderson and E. I. Blount, *Phys. Rev. Lett.* **14**, 217 (1965).
- ⁵⁵L. R. Testardi, *Rev. Mod. Phys.* **47**, 637 (1975); an update of this article was published in the MIR edition (Moscow, U.S.S.R.), 1977.
- ⁵⁶B. Luethi and W. Rehwald, in *Structural Phase Transitions I*, Vol. 23 of *Topics in Current Physics*, edited by K. A. Mueller and H. Thomas (Springer, Berlin, 1981), pp. 131–184.
- ⁵⁷We do not intend to give an extensive list of references on this subject but rather some key references which all come from the Proceedings of the Bat-Sheva Seminar on Electron Density Mapping in Molecules and Crystals that was held at the Weizmann Institute of Science, 1977, edited by F. L. Hirshfeld; K. Kurki-Suonio, *Israel J. Chem.* **16**, 115 (1977); R. F. Stewart, *ibid.* **16**, 124 (1977); P. Coppens, *ibid.* **16**, 159 (1977).
- ⁵⁸S. Ohba, Y. Saito, and S. Wakoh, *Acta Crystallogr. Sect. A* **38**, 103 (1982).
- ⁵⁹J. R. Schneider, N. K. Hansen, and H. Kretschner, *Acta Crystallogr. Sect. A* **37**, 711 (1981), and references therein.
- ⁶⁰A. Freund, *Nucl. Instrum. Methods* **24**, 93 (1975).
- ⁶¹R. Chen, P. Trucano, and R. F. Stewart, *Acta Crystallogr. Sect. A* **33**, 823 (1977).
- ⁶²E. F. Skelton, *J. Appl. Crystallogr.* **2**, 106 (1969).
- ⁶³P. J. E. Aldred and M. Hart, *Proc. R. Soc. London Ser. A* **332**, 223 (1973); *ibid.* **332**, 239 (1973); B. Dawson, in *Advances in Structure Research by Diffraction Methods*, edited by W. Hoppe and R. Mason (Pergamon, Oxford, 1975), Vol. 6.
- ⁶⁴S. Ohba, S. Sato, and Y. Saito, *Acta Crystallogr. Sect. A* **37**, 697 (1981) and references therein.
- ⁶⁵E. Gabe, Y. Le Page, and S. L. Mair, *Phys. Rev. B* **24**, 5634 (1981), and references therein.
- ⁶⁶J. P. Vidal, G. Vidal-Valat, M. Galtier, and K. Kurki-Suonio, *Acta Crystallogr. Sect. A* **37**, 826 (1981), and references therein.
- ⁶⁷E. F. Skelton, S. T. Lin, and G. M. Rothberg, *Acta Crystallogr. Sect. A* **30**, 39 (1974).
- ⁶⁸B. N. Kodess, *Phys. Lett.* **73A**, 53 (1979).
- ⁶⁹A. N. Christensen, *Acta Chem. Scand. Ser. A* **32**, 89 (1978).
- ⁷⁰J.-L. Staudenmann, unpublished results. Least-squares results reported under this reference number concern, of course, refinements for high-order reflections only, that is for reflections with $\sin\theta/\lambda > 0.65 \text{ \AA}^{-1}$ —as in Refs. 13, 30, 33, and 34.